Topological band and superconductivity in math xmlns="http://www.w3.org/1998/Math/MathML">msub>mrow>mi>UTe/mi>/mrow>mn>2/mn>/msub>/math>

Tatsuya Shishidou, Han Gyeol Suh, P. M. R. Brydon, Michael Weinert, and Daniel F. Agterberg

Phys. Rev. B **103**, 104504 — Published 5 March 2021

DOI: 10.1103/PhysRevB.103.104504

Topological band and superconductivity in UTe_2

Tatsuya Shishidou,[1] Han Gyeol Suh,[1] P. M. R. Brydon,[2] Michael Weinert,[1] and Daniel F. Agterberg[1]

[1] *Department of Physics, University of Wisconsin, Milwaukee, WI 53201, USA*
[2] *Department of Physics and MacDiarmid Institute for Advanced Materials and Nanotechnology, University of Otago, P.O. Box 56, Dunedin 9054, New Zealand*

UTe_2 is a likely spin-triplet superconductor that also exhibits evidence for chiral Majorana edge states. A characteristic structural feature of UTe_2 is inversion-symmetry related pairs of U atoms, forming rungs of ladders. Here we show how each rung's two sublattice degrees of freedom play a key role in understanding the electronic structure and the origin of superconductivity. In particular, DFT+U calculations generically reveal a topological band near the chemical potential originating from a band inversion associated with $5f$ electrons residing on these rungs, necessitating a microscopic description that includes these rung degrees of freedom. Furthermore, we show that a previously identified strong ferromagnetic interaction within a U-U rung leads to a pseudospin-triplet superconducting state that accounts for a non-zero polar Kerr angle, the observed magnetic field-temperature phase diagrams, and nodal Weyl fermions. Our analysis may also be relevant for other U-based superconductors.

I. INTRODUCTION

UTe_2[1] is a paradigmatic superconductor exhibiting unconventional behavior: Superconductivity survives to much higher magnetic fields than expected[1–9] and shows a highly unusual re-entrant field induced superconductivity[10]. Furthermore, there is evidence for ferromagnetic fluctuations[11–13], odd-parity superconductivity[14], multiple superconducting phases[15–19], spontaneous broken time-reversal symmetry[16], and chiral Majorana edge and surface states[20,21], the nature of which are not yet understood.

Many important open questions remain, foremost is the origin of the odd-parity superconductivity. There is a consensus that ferromagnetic fluctuations are responsible for the pairing in the related UGe_2, URhGe, and UCoGe compounds,[22] but uncertainty as to the appropriate underlying model has led to debate over the nature of these fluctuations[22]. Recently, this question has been addressed in UTe_2[23–25] where density functional theory plus Hubbard U (DFT+U) and dynamical mean field theory (DMFT) calculations lead to a family of band structures; the consequences of these on superconductivity have been explored, suggesting topological superconductivity[25]. In addition, effective Heisenberg theories developed from an itinerant electron description argue that the strongest magnetic interaction, for all U values considered, is a local ferromagnetic interaction between the two nearest-neighbor U atoms on a ladder rung[24], providing a potential mechanism for superconductivity that does not require a global ferromagnetic ground state.

Here we revisit the DFT+U calculations, finding good agreement with previous results and newly identifying a topological band that appears near the chemical potential for all values of U. This topological band has its origin in the rung sublattice degrees of freedom, in particular, a band inversion between even- and odd-parity $5f$ orbital combinations on the two U atoms of the rung. The nontrivial topological nature implies that *two* Wannier functions localized on the rung sites are needed to describe this band to avoid a topological Wannier obstruction[26]. The appearance of this topological band and the rung ferromagnetic interactions reveal that the rung sublattice degrees of freedom play a central role in the electronic description. Consequently, we construct a symmetry-based electronic model that explicitly includes these rung sublattice degrees of freedom and the ferromagnetic interaction between them. This model yields magnetic field-temperature phase diagrams that agree with experiment, allows a superconducting state with Weyl nodes, and provides an explanation for the observed surface chiral edge states[21], polar Kerr effect[16], and low energy excitations in the superconducting state[27].

II. TOPOLOGICAL BAND

To develop an understanding of the origin of superconductivity in UTe_2, a description of the underlying electron excitations is needed. Here, experiment provides some insight. In particular, the development of Kondo coherence and the size of the superconducting specific heat anomalies[1,2] imply itinerant f-electrons are important. However, a low temperature renormalized Fermi liquid cannot provide a complete description since the magnetic susceptibility for the field along the $\hat{a}$ direction shows a strong upturn at low temperatures[1], inconsistent with a Pauli temperature independent susceptibility expected from a Fermi liquid. Here we take the point of view that this magnetic response is a consequence of quasiparticle interactions which is consistent with the temperature scaling of the magnetic susceptibility[1,13]. Consequently, a natural starting point for the low-temperature electronic structure of UTe_2 is a renormalized interacting Fermi liquid in which U $5f$ electrons participate, which is also consistent with scanning tunneling microscopy[21] and the observed Fermi pocket about the X-point seen in ARPES data[28,29] (called Z in Ref. 29). This point of view has been adopted in recent

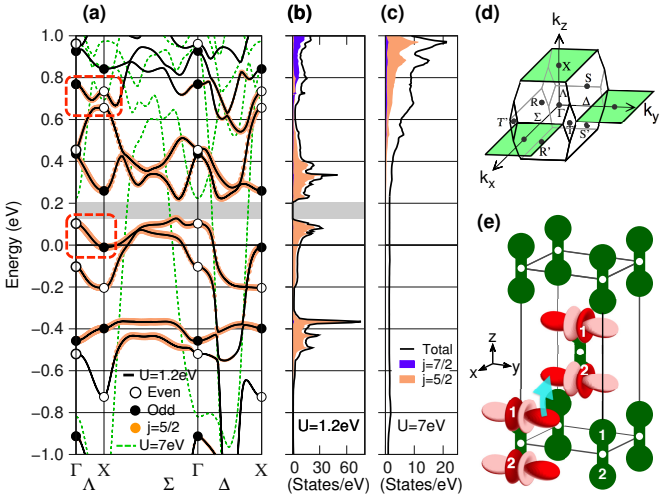

FIG. 1. (a) DFT+U bands for U=1.2 eV (black solid lines) and 7 eV (green dotted lines). For the former, the f j=5/2 component (orange) and even/odd parities (open/closed circles) are shown. A 81 meV band gap (grey shaded region) separates a pair of topological $5f$ bands, indicated by red-dotted boxes along the Λ direction. Density of states for (b) U=1.2 eV and (c) 7 eV. (d) First BZ, with eight TRIMs and equivalent X faces (green) shown; all three principal k lines (Λ, Σ, and Δ) connect Γ and X. (e) Wave function schematics of topological band at X point with odd parity. Thin/thick shading of lobes represents their positive/negative sign. In accord with the wave vector k=(0,0,2π), the sign array of body-centered orbitals is reversed from that of corner-centered. The inter-rung U(1)-U(2) bonding (blue arrow) is retained at the Γ point as well.

DMFT and DFT+U calculations[23–25]. The band structure depends strongly on the choice of U, suggesting that any theory of the superconducting state needs to be developed for a range of band structures, emphasizing properties that are generic across the relevant possibilities. Here, we have carried out DFT calculations of the band structure of UTe_2 using the full-potential linearized augmented plane wave method[30] and including a Coulomb U to account for interactions of the U $5f$ electrons[31]. Our results agree with those found earlier[24,25]. A key new finding is that for a wide range of U, we find a topological band at or near the chemical potential.

As reported earlier, the band structure differs significantly along the three principal k axes due to the underlying quasi one-dimensional (1D) bands; these features are most easily seen in the no-$5f$ limit or, equivalently, in the large U limit, c.f., Fig. 1(a). The quasi-1D bands arise from the U $6d$ dimer state, which strongly disperses along the k_x (Σ) direction, and also the Te $5p$ linear chain state which disperses along the k_y (Δ) direction. For realistic values of U (e.g., U = 1.2eV in Fig. 1(a)), the $5f$ states are able to hybridize with these bands, leading to rather complicated dispersions along Σ and Δ. In contrast, the $5f$ dispersion along k_z (Λ) is much simpler and we can make the following observations for the j=5/2 sector: (i) Among the six Kramers-degenerate bands, two are *topologically nontrivial* in the sense that the band parity switches between Γ and X, while the other four bands do not show such a parity change; (ii) these two are well separated in energy; (iii) the lower energy band, located near the chemical potential (energy zero), has even parity at Γ and odd at X; and (iv) of the four trivial bands, a set of odd- and even-parity bands are occupied.

These features persist regardless of U. The band structure and density of states (DOS), Figs. 1(b)(c), however, constrain the range of U that reproduce the experimental results such as the strong ARPES signals around −0.5 eV[28] or −0.7 eV[29]. In particular, for a range of moderate U (1.1–2.0 eV), a band gap appears just above the lower nontrivial band; the Hilbert space below this gap (corresponding to the occupied levels of a $+2e$ doped system) is characterized by Z_2 topological invariants $(\nu_0;\nu_1,\nu_2,\nu_3)$[32], which are found from the band parities at the eight time-reversal-invariant momenta (TRIMs). Due to a mirror symmetry duplication of R, S, and T [c.f., Fig. 1(d)], the index ν_0 is determined solely from the parity products at Γ and X, $(-1)^{\nu_0} = \delta_\Gamma\delta_X$ for our choice of origin. The $5f$ band with nontrivial parity switching leads to a strong topological state ν_0=1. The other indices are all identical, ν_1=ν_2=ν_3=1, determined from $(-1)^{\nu_1} = \delta_X\delta_R\delta_S\delta_T$. In a smaller U range that includes U=0 eV, the non-doped system now has a genuine insulating band gap where exactly the same $5f$ band provides ν_0=1. This topological $5f$ band consists predominantly of $y(5y^2-3r^2)$ orbitals on each of the two U atoms forming a rung (note these orbitals are hybridized with Te $5p$ orbitals). At Γ, the wave function has opposite sign on these two atoms, and hence has even parity; however, as sketched in Fig. 1(e), at the X point the wave function has the same sign on the two rung atoms and is therefore odd parity. Common to these states at Γ and X is the U(1)-U(2) bond that connects different rungs. For the U used here (1.2 eV), this topological band gives rise to a Fermi surface that is centered on the X-point, in agreement with the Fermi pocket observed experimentally[28,29]. More details of the band structure analysis, including the U dependence, are in the Appendices.

III. MINIMAL SINGLE BAND HAMILTONIAN

The observation that the band nearest to the chemical potential is topological has important consequences for constructing an effective theory of the superconducting state. This is not restricted to the possible interplay of the normal state topological edge states and odd-parity superconducting edge states[33]. Rather, a minimal model to describe the band nearest the chemical potential and its superconductivity requires *two* Wannier functions, each localized on one of the two rung sublattice degrees of freedom. This is necessary to avoid a Wannier obstruction[26]. Surprisingly, this U atom sublattice

rung degree of freedom has not been explicitly considered previously in understanding the low-energy physics and superconducting state in UTe_2, nor in the related materials UGe_2, URhGe, and UCoGe where a similar U sublattice structure appears[22]. Here we consider the role of this sublattice degree of freedom through the construction of a minimal model. In particular, motivated by the DFT+U results, we assume Wannier functions centered on the U sites encode the low energy electronic excitations. These Wannier functions will in general consist of U f-electron states hybridized with Te $5p$ states. The U atoms sit on sites of C_{2v} symmetry, for which only a single spinor symmetry representation exists. A minimal model therefore includes a single spinor pair centered on each of the sublattices. While these spinors share the same symmetry properties as usual spin-1/2 fermions under C_{2v} symmetry, DFT reveals they are generally a linear combination of j=5/2 states (hybridized with Te $5p$ orbitals). This model includes two bands and we assume only one of these cross the chemical potential. This is consistent with ARPES measurements that observe only one Fermi pocket associated with the U $5f$ electrons[29], which are responsible for the superconducting state, suggesting this model is a reasonable description. The most general non-interacting Hamiltonian including all symmetry-allowed terms with sublattice and spin degrees of freedom is

$$\begin{aligned} H_N =&\epsilon_0(k) - \mu + f_{A_g}(k)\tau_x + f_z(k)\tau_y + f_y(k)\sigma_x\tau_z \\ &+f_x(k)\sigma_y\tau_z + f_{A_u}(k)\sigma_z\tau_z \end{aligned} \quad (1)$$

where the functions $f_i(k)$ have symmetry properties given by the label i: $f_{A_g}(k) \sim$ constant, $f_z(k) \sim k_z$, $f_y(k) \sim k_y$, $f_x(k) \sim k_x$, and $f_{A_u}(k) \sim k_x k_y k_z$. Here the Pauli matrices σ_i (τ_i) describe the spin (rung) degrees of freedom. While our analysis below does not depend upon the detailed form of the $f_i(k)$, for the $y(5y^2 - 3r^2)$ Wannier functions discussed above we obtain the following tight-binding theory:

$$\begin{aligned} \epsilon_0(k) &= t_1 \cos(k_x) + t_2 \cos(k_y) \\ f_{A_g}(k) &= m_0 + t_3 \cos(k_x/2)\cos(k_y/2)\cos(k_z/2) \\ f_z(k) &= t_z \sin(k_z/2)\cos(k_x/2)\cos(k_y/2) \\ f_y(k) &= t_y \sin(k_y) \\ f_x(k) &= t_x \sin(k_x) \\ f_{A_u}(k) &= t_u \sin(k_x/2)\sin(k_y/2)\sin(k_z/2)\ . \end{aligned} \quad (2)$$

To replicate the nontrivial parity switching predicted above, the magnitude of the *inter-rung* U(1)-U(2) hopping t_3 [see Fig. 1(e)] needs to exceed the *intra-rung* hopping m_0. Fitting to the DFT+U topological band gives $(\mu, t_1, t_2, m_0, t_3, t_z, t_x, t_y, t_u) = (-0.129, -0.0892, 0.0678, -0.062, 0.0742, -0.0742, 0.006, 0.008, 0.01)$ and yields the Fermi surface shown in Fig 3.

IV. QUASIPARTICLE INTERACTIONS

Following spin-fluctuation theory[34,35], we assume that magnetic correlations among the quasiparticles drive superconductivity. To gain insight into the nature of these interactions, we use recent DFT + U results that find lowest energy FM and AFM states[24] using a Heisenberg-like description of itinerant electron magnetic states. A relevant result is that the largest magnetic interaction is a local ferromagnetic interaction between the rung degrees of freedom, the lowest energy FM and AFM configurations are consistent with this local configuration[24] and may account for the two magnetically-ordered states observed experimentally[17]. Consistent with these DFT +U results, we assume that the dominant quasiparticle interaction is

$$H_{int} = -\sum_i (J_x S^x_{i,1} S^x_{i,2} + J_y S^y_{i,1} S^y_{i,2} + J_z S^z_{i,1} S^z_{i,2}) \quad (3)$$

where $1, 2$ labels the two U atoms on the rung, i labels a lattice point, and S_i is the local quasiparticle spin; the ferromagnetic interactions $J_\mu > 0$ are in general unequal due to the orthorhombic structure. Treating this as an effective coupling for superconductivity, we find three possible pairing states as listed in Table I. Due to the inter-sublattice nature of the magnetic interactions, the gap functions are necessarily proportional to a non-trivial τ_y sublattice operator and take the form $\Delta_i \tau_y \sigma_i$ which describes a local, inter-sublattice, spin-triplet pairing function. While the interactions reveal the role of magnetic anisotropy on the pairing, we will now set $J_x = J_y = J_z$ to examine the effect of H_N on these pairing states.

TABLE I. Pairing gap functions due to ferromagnetic interactions between rung sublattice degrees of freedom. The first column gives the local gap function and the last column gives the corresponding $\vec{d}(k)$ in the band basis when the spin-orbit coupling terms are vanishing ($f_x = f_y = f_{A_u} = 0$), with the abbreviation $\widetilde{f}_z(k) = f_z(k)/\sqrt{f^2_{A_g}(k) + f^2_z(k)}$.

Gap	Irrep	Interaction	Momentum dependence
$\Delta_z \tau_y \sigma_z$	A_u	$J_x + J_y - J_z$	$\widetilde{f}_z(k)\,\hat{z}$
$\Delta_x \tau_y \sigma_x$	B_{2u}	$-J_x + J_y + J_z$	$\widetilde{f}_z(k)\,\hat{x}$
$\Delta_y \tau_y \sigma_y$	B_{3u}	$J_x - J_y + J_z$	$\widetilde{f}_z(k)\,\hat{y}$

A. Role of H_N

Naively, the stable pairing state is determined by the largest interaction parameter listed in Table I. However, due to the spin-sublattice coupling in our model, H_N also influences the relative stability of the pairing states. The effect of the distinct terms in H_N on the transition temperature $T_{c,i}$ of the state $\Delta_i \tau_y \sigma_i$ can be quantified without fully specifying the functions $f_j(k)$ using the concept of superconducting fitness[36,37]: specifically, if the matrix $\sigma_i \tau_j$ commutes with the gap function $\Delta_i \tau_y \sigma_i$, then the corresponding term in H_N will enhance $T_{c,i}$; conversely, $T_{c,i}$ is suppressed by this term if it anticommutes with the pairing potential[37]. This yields the result that the f_{A_g}

term suppresses all the $T_{c,i}$ and the f_z term enhances all the $T_{c,i}$. Consequently, if $J_x = J_y = J_z$, the spin-orbit coupling terms will dictate which $T_{c,i}$ is highest. In particular, the largest $T_{c,i}$ is given by the smallest of $\langle f_{A_u}^2 \rangle$ (A_u stable), $\langle f_x^2 \rangle$ (B_{3u} stable), or $\langle f_y^2 \rangle$ (B_{2u} stable), where $\langle \ldots \rangle$ represents an average over the Fermi surface. The terms in the tight-binding expression will be altered by pressure, providing a potential explanation for the appearance of different superconducting states.

H_N also dictates the form of the pseudospin triplet $\vec{d}$-vector on the Fermi surface. We do not give the details here but point out that generically, all three pseudospin components $\hat{x}, \hat{y}, \hat{z}$ appear for each gap function. As we argue below, there is one limit that can be motivated by experimental results. In particular, when the momentum-dependent spin-orbit coupling terms are small, that is f_x^2, f_y^2, $f_{Au}^2 << f_z^2$ then the orientation of the spin-triplet $\vec{d}$ vectors is set by the spin part of the gap function in Table I. In this case Table I provides an approximately correct description of $\vec{d}$ (except near $k_z = 0, 2\pi$); in the following this is called the weak spin-orbit coupling limit.

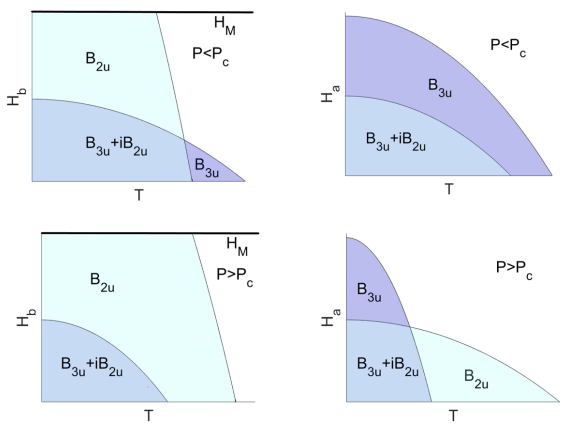

FIG. 2. Qualitative temperature-field phase diagrams for fields along the $\hat{a}$ and $\hat{b}$ directions. The top two phase diagrams correspond to $P < 0.2$ GPa and the bottom two to $P > 0.2$ GPa. H_M corresponds to an observed metamagnetic transition.

B. Relationship to experiment

At ambient pressure, two superconducting transitions in zero field and a polar Kerr effect that can be trained by a c-axis magnetic field have been observed[16]. The latter result implies a $B_{3u} + iB_{2u}$ or a $A_u + iB_{1u}$ pairing below the second transition[16]. In the context of our theory, the only possibility is the $B_{3u} + iB_{2u}$ state. Such a broken-time reversal symmetry state can be stabilized by ferromagnetic fluctuations[16,38,39]. Assuming an isotropic rung exchange, this situation arises in our model by requiring that $\langle f_x^2 \rangle < \langle f_y^2 \rangle < \langle f_{A_u}^2 \rangle$.

The weak spin-orbit coupling limit is consistent with the field-dependence of the phase diagram for fields along $\hat{a}$ and $\hat{b}$ as a function of pressure[15,17,40,41]. In this limit the B_{3u} gap is primarily along $\hat{b}$ and the B_{2u} gap is primarily along $\hat{a}$, implying that the B_{3u} (B_{2u}) gap will experience paramagnetic limiting for a field along $\hat{b}$ ($\hat{a}$) and not for the fields along $\hat{a}$ ($\hat{b}$). It has been observed that the two superconducting transitions cross at a critical pressure $P_c \approx 0.2$ GPa[17]. In our model such a crossing should then be correlated with a switch in the upper critical field behavior for the field along the $\hat{a}$ and $\hat{b}$ directions, as shown in Fig. 2. This is indeed what is observed[1,40,41].

In addition, the weak spin-orbit coupling limit naturally explains why thermal conductivity exhibits nodal behavior that is similar along both the $\hat{a}$ and $\hat{b}$ directions[27]: When $f_x = f_y = f_{A_u} = 0$, all the gap functions have accidental line nodes when $k_z = 0$, yielding nodal thermal conductivity behavior along both $\hat{a}$ and $\hat{b}$. These accidental line nodes will be lifted when the spin-orbit coupling terms are non-zero, but if they are small we expect a local gap minimum near $k_z = 0, 2\pi$ which can mimic nodes in thermal conductivity.

C. Weyl Nodes

Using the tight-binding theory given above, we find that Weyl nodes generically exist for a $B_{3u} + iB_{2u}$ pairing state. These nodes are topologically protected but do not sit at high symmetry positions, instead the positions are determined by the relative amplitudes of the B_{2u} and the B_{3u} order parameters. The evolution of these nodes is shown in Fig. 3. We have also computed the Weyl charge of these nodes. Generically, there exists four Weyl nodes, two of charge $+1$ and two of charge -1. These Weyl nodes imply the existence of surface arc states which provide an explanation for the chiral edges states seen with scanning tunneling microscopy[21].

D. Polar Kerr Effect

Our multiband theory generically gives rise to an imaginary anomalous Hall conductivity, which is expected to be proportional to the polar Kerr signal. By a sum rule[42] we have that the integrated imaginary anomalous Hall conductivity is given by $\int_{-\infty}^{\infty} \omega \, \mathrm{Im}\{\sigma_H(\omega)\} d\omega = -i\pi e^2 \langle [\partial_{k_x} H_N, \partial_{k_y} H_N] \rangle$. The full expansion of the commutator is very complicated and will be analyzed elsewhere, but we note that the contribution $(\partial_{k_x} f_y \partial_{k_y} f_x - \partial_{k_x} f_x \partial_{k_y} f_y)\sigma_z \tau_0$ is directly proportional to the so-called time-reversal-odd bilinear of the $B_{3u} + iB_{2u}$ pairing state[43,44]. This implies that expectation value of the commutator is nonzero, ensuring the existence of the anomalous Hall conductivity and hence the polar Kerr signal. The presence of two bands due to the sublattice degree of freedom is critical; in a single-band model, the

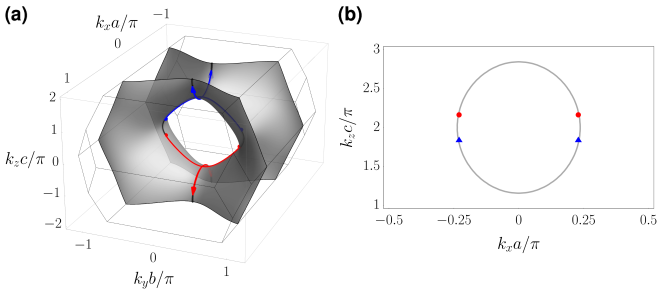

FIG. 3. (a) Evolution of Weyl nodes of $B_{2u} + iB_{3u}$ pairing states as the relative amplitude of the B_{2u} gap to the B_{3u} gap is reduced. The gap amplitudes are chosen to be $(\Delta_x, \Delta_y) = 1\text{meV}(\cos\theta, \sin\theta)$ where θ is a real parameter. The total gap intensity 1meV is chosen small enough to keep the Weyl nodes close to the normal state Fermi surface. Making this intensity smaller does not change the qualitative behavior of the Weyl nodes. The Fermi surface is obtained from the tight-binding model fitted to the two DFT+U bands with U=1.2 eV. Red and blue lines indicate trajectories of the nodes with +1 and −1 Weyl charge. There are four nodes in a Brillouin zone and they sit on the k_x-k_z or k_y-k_z plane. Two pairs with a same charge sign meet at the k_z axis when $\theta = \pi/4$. (b)Weyl points on k_x-k_z slice when $\theta = 0.254\pi$. Triangles (blue) and circles (red) indicate +1 and −1 Weyl charge. The circular line is a cut of the Fermi surface and centered at the X-point.

commutator is vanishing, and a polar Kerr effect does not appear in the clean limit[45].

V. CONCLUSIONS

From DFT+U calculations, we have identified a topological band near the chemical potential in UTe_2 that stems from U $5f$ electrons. This result, together with the importance of rung ferromagnetic interactions, suggests that U atom rung degrees of freedom play an important role in the superconductivity of UTe_2. We have developed a model that includes these degrees of freedom and captures the topological bands. In addition, we show that including the ferromagnetic rung interactions allows a $B_{3u} + iB_{2u}$ pairing state, accounting for Polar Kerr measurements and yielding Weyl points, providing a promising model with which to understand UTe_2 in more detail. Similar U sublattice degrees of freedom exist in UGe_2, URhGe, and UCoGe, suggesting a unifying motif for this class of materials.

ACKNOWLEDGMENTS

We acknowledge useful discussions with Nick Butch, Yun Suk Eo, Ian Hayes, Aharon Kapitulnik, Johnpierre Paglione, Srinivas Raghu, and Didi Wei. This work was supported by the U.S. Department of Energy, Office of Basic Energy Sciences, Division of Materials Sciences and Engineering under Award DE-SC0017632. H.G.S. was supported by the University of Wisconsin-Milwaukee through the Distinguished Graduate School Fellowship. P.M.R.B. was supported by the Marsden Fund Council from Government funding, managed by Royal Society Te Apārangi.

Appendix A: Details of DFT calculations

DFT calculations of UTe_2 were carried out by the full-potential linearized augmented plane wave method[30]. The experimentally determined lattice parameters[11] are used: space group $Immm$; a =4.1611, b =6.1222, c =13.955 Å with fractional coordinates (0, 0, 0.13544), (0.5, 0, 0.29750), (0, 0.2509, 0.5) for the U $4i$ site, Te $4j$ and $4h$ sites, respectively. The muffin-tin sphere radii are set to 1.35 Å, and the wave function and potential cutoffs are 16 and 100 Ry, respectively. The Brillouin zone is sampled with a 15×15×15 k-point mesh during the self-consistent field cycle. To account for the Coulomb correlation in U $5f$ states, a rotationally invariant version of the local density approximation plus Hubbard U (LDA+U) method[31] is employed, with the full 14 × 14 5f occupation matrix and the Slater integrals other than monopole term $F_0 = U$ are set to zero[25].

It has been demonstrated that varying U causes drastic changes to the Fermi surface (FS) of UTe_2, including an insulator-metal transition, FS volume change, and more importantly, a FS topological Lifshitz transition[25]. We reexamine here the U dependency, detecting the FS trend

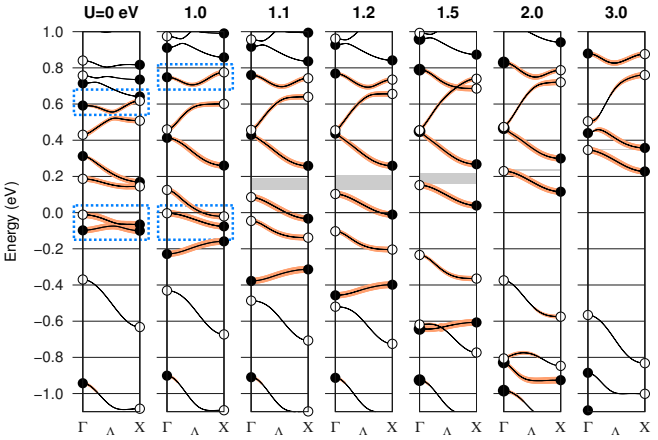

FIG. 4. DFT+U band dispersion along the Λ line connecting the Γ and X (Z) points. Results with U varied from 0 eV (pure LDA) to 3 eV are shown. Bands with substantial U $5f$ j=5/2 components are indicated by orange. Band even/odd parity is given by open/closed circle. Around −0.5 eV, there is an even-parity band that has its origin in the dimerization of U $6d$ z^2 orbitals within a two-U rung. The bands near and below −1 eV are dominated by Te $5p$ states. A pair of $5f$ bands that show nontrivial parity switching are found to exist in the j=5/2 manifold regardless of U; for U=0 and 1 eV, these are marked by blue dotted line.

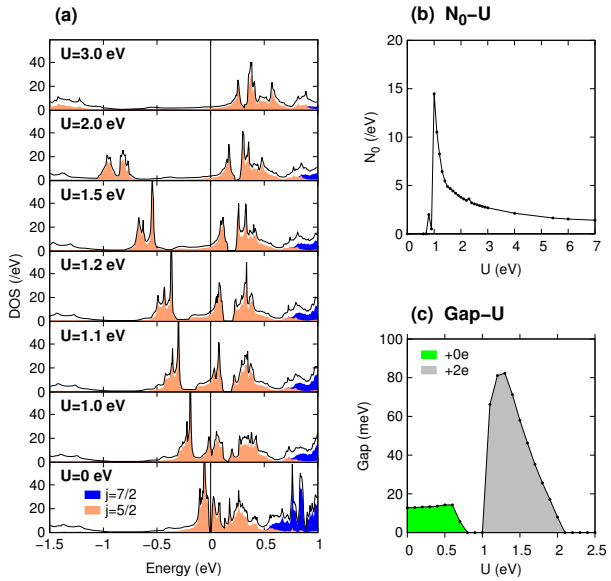

FIG. 5. U dependence of (a) density of states, (b) chemical-potential density of states, and (c) two types of band gap; non-doped gap (green) and $+2e$ doped gap (grey).

addressed before as well as finding important aspects for the topological $5f$ band that is the focus of main text.

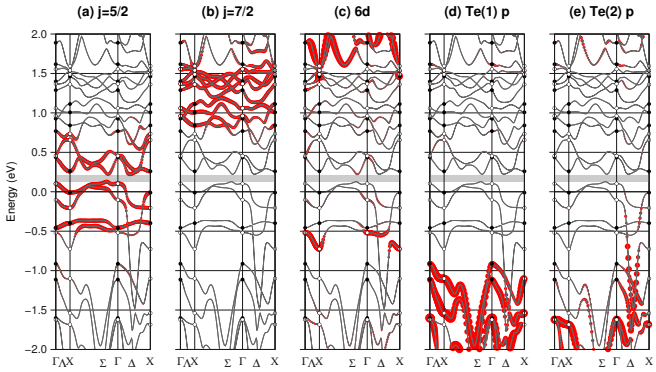

FIG. 6. Λ-Σ-Δ band dispersion (U=1.2 eV) in the energy range ±2 eV about the chemical potential. Each of five panels shows different components of the wave function with a fat-band representation (red) laid on top of the same band dispersion plot (black lines). (a) and (b): U $5f$ $j = 7/2$ and $j = 5/2$ components, respectively. (c) U $6d$, (d) Te $4j$ site $5p$, and (e) Te $4h$ site $5p$ component.

Figure 4 shows the U variation of Λ-line band dispersion. Around the chemical potential (energy zero), there is a $5f$ band that changes its parity from even (Γ) to odd (X), which persists for all values of U (including larger ones not shown here). At U=0 eV (pure LDA), two entangled $5f$ bands are in the occupied levels; one is trivial with odd parity (located around −0.1 eV) and the other is the nontrivial band. There is a tiny insulating bandgap of 13 meV. Above that, there is a trivial even-parity band around 0.2 eV. Turning on U, these two trivial bands shift down to deeper binding. At U=1.1 eV, the energy ordering between the topological band and the even-parity band is reversed compared to smaller U values, which corresponds to the Fermi-surface Lifshitz transition addressed in Ref. 25 that accompanies a drastic increase of FS volume. The electron pocket thus made by the topological $5f$ band at X and along the Λ line exists in a limited range of U values, 1.1 eV $\leq U \leq$ 1.3 eV, since this band is pushed upward with increasing U, producing a hole pocket along k_y direction from X, which eventually becomes the large FS led by the quasi one-dimensional Te $5p$ band[25]. Although the energy position of the $5f$ bands is sensitive to U, Fig. 4 shows that the band closest in energy to the chemical potential at X is the topological $5f$ band.

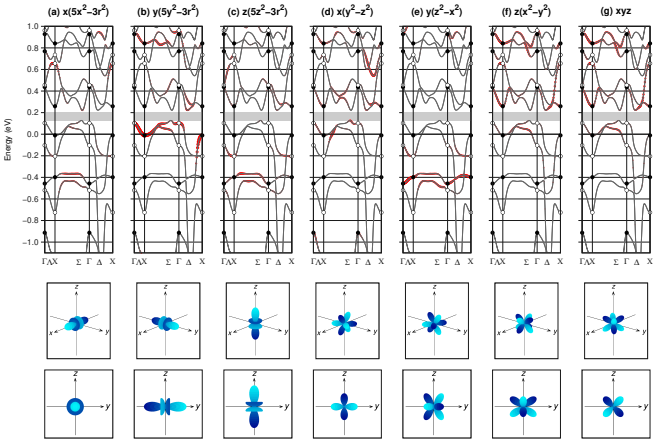

FIG. 7. Upper panels: Λ-Σ-Δ band dispersion (U=1.2 eV) in the energy range ±1 eV with atomic U $5f$ component projection onto the $\ell = 3$ cubic harmonics shown by red dots. The topological band around the chemical potential has predominantly $T_{1y} = y(5y^2 - 3r^2)$ orbital character. Lower panels: three-dimensional and two-dimensional (y-z planar) schematic view of the $\ell = 3$ cubic harmonics.

Figure 5(a) shows the variation in the density of states

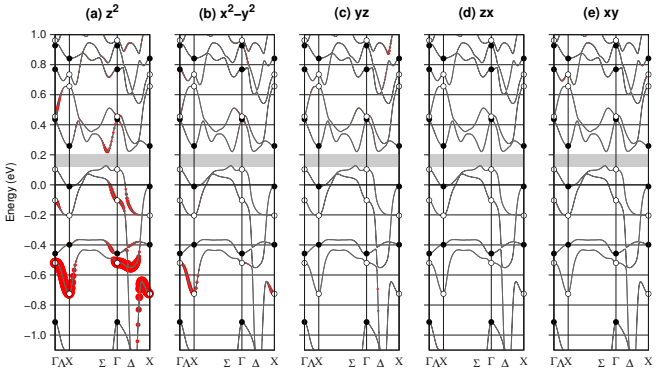

FIG. 8. Λ-Σ-Δ band dispersion (U=1.2 eV) with the atomic U $6d$ component projected onto $\ell = 2$ cubic harmonics shown by red dots.

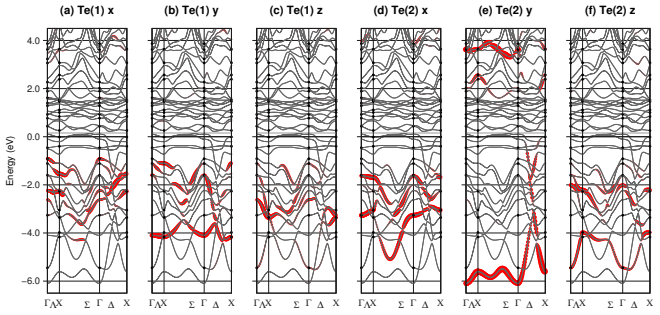

FIG. 9. Λ-Σ-Δ band dispersion (U=1.2 eV) with the Te atomic $5p$ component (x, y, and z) shown by red dots. Note that the energy range displayed is much wider than that of the other figures to accommodate the large bonding-antibonding splitting of Te(2) p_y state. Te(1) and (2) are abbreviation for the Te site $4j$ and $4h$, respectively. Note as well that even-parity symbols are dropped.

(DOS) with U. For moderate U, 0 eV $\leq U \leq$ 2 eV, a strong peak in the occupied levels goes to the deeper binding energy as U is increased. The photoemission spectroscopy found intense $5f$-originated signals around 0.5 eV[28] and 0.7 eV[29], which may be explained by this peak. The DOS at the chemical potential, N_0, is zero for U=0 eV because of an insulating band gap. As shown in Fig. 5(b), N_0 is a drastic function of U with a large peak around U=1 eV, which reflects the fact that the topological $5f$ band located in the occupied levels at U=0 eV moves up in energy as U increases and passes through the chemical potential; for higher U, N_0 continuously declines by losing $5f$ contributions. The formation of a band gap is seen in Fig. 5(a) and its size is shown in Fig. 5(c) as a function of U. For small U ($\leq$ 0.8 eV), an insulating gap ∼13 meV exists. After this gap closes with increasing U, another gap is formed just above the topological $5f$ band, which corresponds to an insulating gap for $+2e$ doped system. This gap exists for U in the range 1.1 eV $\leq U \leq$ 2 eV, with a maximum of 82 meV at U=1.3 eV.

For the two U ranges of Fig. 5(c) that have a band gap, Z_2 topological invariants $(\nu_0; \nu_1, \nu_2, \nu_3)$ are examined by calculating the band parity product below the band gap at the eight TRIM points. The parity product arrays $(\delta_\Gamma, \delta_X, \delta_R, \delta_S, \delta_T, \delta_{R'}, \delta_{S'}, \delta_{T'})$ is found to be invariant within each of the U ranges and is shown in Table II. This gives the Z_2 invariants (1; 1,1,1) for both U ranges.

We analyze wave function component in terms of atomic-like orbitals. Within muffin-tin spheres, partial ℓ wave is projected onto cubic harmonics. In Figures 6, 7, 8, 9, this atomic-orbital weight is provided in the fat band representation along the Λ-Σ-Δ line.

Appendix B: Choice of origin and parity

For a system with inversion symmetry, the choice of origin can affect the parity label of a state, but will not affect the topological Z_2 invariant. For a lattice choice $\boldsymbol{R} = \sum n_i \boldsymbol{a}_i$ the TRIM points are $\boldsymbol{k}_p = \boldsymbol{G}_p/2$ where $\boldsymbol{G}_p = \sum m_j \boldsymbol{b}_j$ with $n_j = 0, 1$, where $\boldsymbol{a}_i$ and $\boldsymbol{b}_j$ are the primitive direct and reciprocal lattice vectors, respectively. For a lattice vector $\boldsymbol{R} = \sum n_i \boldsymbol{a}_i$, translational symmetry (Bloch's theorem) requires that

$$\{\, e|\boldsymbol{R}\}^{-1} \psi_{\boldsymbol{k}}(\boldsymbol{r}) = \psi_{\boldsymbol{k}}(\{\, e|\boldsymbol{R}\}\boldsymbol{r}) = e^{i\boldsymbol{k}\cdot\boldsymbol{R}} \psi_{\boldsymbol{k}}(\boldsymbol{r}).$$

If $\boldsymbol{k} = \boldsymbol{k}_p$, then $e^{i\boldsymbol{k}_p\cdot\boldsymbol{R}} = e^{i\boldsymbol{G}\cdot\boldsymbol{R}/2} = \pm 1$. At a TRIM point, inversion is an operation of the group of $\boldsymbol{k}_p$, and hence if the origin is at an inversion center,

$$\{\, i|0\}\, \psi_{\boldsymbol{k}_p}(\boldsymbol{r}) = \psi_{\boldsymbol{k}_p}(-\boldsymbol{r}) = \lambda\, \psi_{\boldsymbol{k}_p}(\boldsymbol{r}), \quad \lambda = \pm 1, \tag{B1}$$

where λ is the parity. With a shift of the origin to $\boldsymbol{r}_o$, $\boldsymbol{r}' = \boldsymbol{r} - \boldsymbol{r}_o = \{\, e|\boldsymbol{r}_o\}^{-1}\, \boldsymbol{r}$, a wave function relative to the new origin is

$$\psi_{\boldsymbol{k}}(\boldsymbol{r}') = \psi_{\boldsymbol{k}}(\{\, e|\boldsymbol{r}_o\}^{-1}\boldsymbol{r}) = \{\, e|\boldsymbol{r}_o\}\, \psi_{\boldsymbol{k}}(\boldsymbol{r}),$$

and still transforms under translations as $\boldsymbol{k}$. Applying $\{\, e|\boldsymbol{r}_o\}$ to the right-hand side of Eq. (B1), gives

$$\lambda\, \{\, e|\boldsymbol{r}_o\}\, \psi_{\boldsymbol{k}_p}(\boldsymbol{r}) = \lambda\, \psi_{\boldsymbol{k}_p}(\boldsymbol{r}'), \tag{B2}$$

and to the left-hand side

$$\begin{aligned} \{\, e|\boldsymbol{r}_o\}\, \{\, i|0\} \psi_{\boldsymbol{k}_p}(\boldsymbol{r}) &= \{\, e|\boldsymbol{r}_o\}\, \{\, i|0\}\, \{\, e|\boldsymbol{r}_o\}^{-1}\, \{\, e|\boldsymbol{r}_o\}\, \psi_{\boldsymbol{k}_p}(\boldsymbol{r}) \\ &= \{\, e|\boldsymbol{r}_o\}\, \{\, i|0\}\, \{\, e|\boldsymbol{r}_o\}^{-1}\, \psi_{\boldsymbol{k}_p}(\boldsymbol{r}') \\ &= \{\, i|2\boldsymbol{r}_o\}\, \psi_{\boldsymbol{k}_p}(\boldsymbol{r}') \end{aligned} \tag{B3}$$

The new origin is also a center of inversion if $\boldsymbol{r}_o$ is half a lattice vector, $\boldsymbol{r}_o = \boldsymbol{R}/2$, and $\{\, i|\boldsymbol{R}\}$ is then a product of inversion and translation. Thus, the left-hand side becomes

$$\begin{aligned} \{\, i|\boldsymbol{R}\}\, \psi_{\boldsymbol{k}_p}(\boldsymbol{r}') &= \{\, i|0\}\, \{\, e|\boldsymbol{R}\}^{-1}\, \psi_{\boldsymbol{k}_p}(\boldsymbol{r}') \\ &= \{\, i|0\}\, e^{i\boldsymbol{k}_p\cdot\boldsymbol{R}} \psi_{\boldsymbol{k}_p}(\boldsymbol{r}') \\ &= e^{i\boldsymbol{k}_p\cdot\boldsymbol{R}}\, \{\, i|0\}\, \psi_{\boldsymbol{k}_p}(\boldsymbol{r}')\ . \end{aligned} \tag{B4}$$

Combining Eqs. (B2) and (B4) (and rearranging),

$$\{\, i|0\}\, \psi_{\boldsymbol{k}_p}(\boldsymbol{r}') = e^{-i\boldsymbol{k}_p\cdot\boldsymbol{R}}\, \lambda\, \psi_{\boldsymbol{k}_p}(\boldsymbol{r}') = \pm\lambda\, \psi_{\boldsymbol{k}_p}(\boldsymbol{r}'). \tag{B5}$$

This means that the parity of the wave functions at the TRIM depends on the choice of origin, differing by a factor of $e^{i\boldsymbol{k}_p\cdot\boldsymbol{R}} = \pm 1$ for all wave functions at a given TRIM point. Then for the 8 TRIM points and $\boldsymbol{r}_o = \boldsymbol{R}/2 = \sum(n_i/2)\, \boldsymbol{a}_i$, the change in parity is:

$$\begin{aligned} \boldsymbol{G}_p \quad &: e^{i\boldsymbol{k}_p\cdot\boldsymbol{R}} \\ (0,0,0)\ &: 1 \\ (1,0,0) &: (-1)^{n_1} \\ (0,1,0) &: (-1)^{n_2} \\ (0,0,1) &: (-1)^{n_3} \\ (0,1,1) &: (-1)^{n_2+n_3} \\ (1,0,1) &: (-1)^{n_1+n_3} \\ (1,1,0) &: (-1)^{n_1+n_2} \\ (1,1,1) &: (-1)^{n_1+n_2+n_3} \end{aligned}$$

TABLE II. Parity product at each of the eight TRIMs $\Gamma_i = (1/2)(n_1\boldsymbol{b}_1 + n_2\boldsymbol{b}_2 + n_3\boldsymbol{b}_3)$. Our choice of primitive vectors is $\boldsymbol{b}_1 = (0,1,1)$, $\boldsymbol{b}_2 = (1,0,1)$, $\boldsymbol{b}_3 = (1,1,0)$ in units of the conventional reciprocal lattice vectors $\boldsymbol{a}^*$, $\boldsymbol{b}^*$, $\boldsymbol{c}^*$. The inversion center that defines the parity is set to the lattice point at the origin. Results are shown for two U ranges, where a band gap is formed at the chemical potential for either $+0e$ or $+2e$ doping.

TRIM	Γ	X	R	S	T	R′	S′	T′
(n_1, n_2, n_3)	(0,0,0)	(1,1,1)	(0,1,0)	(1,0,0)	(0,0,1)	(1,0,1)	(0,1,1)	(1,1,0)
Conventional	(0,0,0)	(0,0,1)	(1,0,1)/2	(0,1,1)/2	(1,1,0)/2	(1,0,−1)/2	(0,1,−1)/2	(1,−1,0)/2
$0 \le U \le 0.8$ $(+0e)$	+	−	−	−	−	−	−	−
$1.1 \le U \le 2$ $(+2e)$	+	−	−	+	+	−	+	+

The Z_2 is the product of these changes, which is $(-1)^{4(n_1+n_2+n_3)} = 1$, i.e., it is independent of the choice of origin. The choice of origin used in the paper allowed the discussion to be completely in terms of the parity at Γ and X. Using an origin at $(\frac{1}{4},\frac{1}{4},\frac{1}{4})$ in terms of the conventional cell, changes the parity of the states at X, which is compensated by the fact that the states at R and R' no longer have the same parity; this behavior is related to the fact that the mirror plane is not through this origin.

Appendix C: Tight-binding model fit to DFT band

Our tight-binding (TB) model is written as Eq. (1-2) in the main text by nine parameters $(\mu, t_1, t_2, m_0, t_3, t_z, t_x, t_y, t_u)$. First we select the $5f$ electron topological band participating in the Fermi surface (FS) formation. Since the other paired topological band is above the chemical potential we also select a lower energy band from the TB model. To obtain a model capturing physics near the FS we fit the TB model's lower energy band to the DFT band with weighting factor $1/(|\epsilon| + \epsilon_0)$ where ϵ is a band energy and we set ϵ_0 to be 0.033eV. Also we set momentum sampling points on Λ-Σ-Δ and Γ-R-W-S line. Guided by a Slater-Koster two center approximation, we take $t_3 = -t_z$. The Γ-R-W-S line is needed to fix t_x, t_y, and t_u because they are vanishing or small on high symmetry lines, as an example the t_u term is zero everywhere on Λ-Σ-Δ. The band dispersion of the fitted TB model is shown in Fig. 10. A comparison between 3D FS shapes for the tight binding theory and the DFT $+U$ results is also shown in Fig. 11, showing that our simple tight binding theory qualitatively captures the Fermi surface shape.

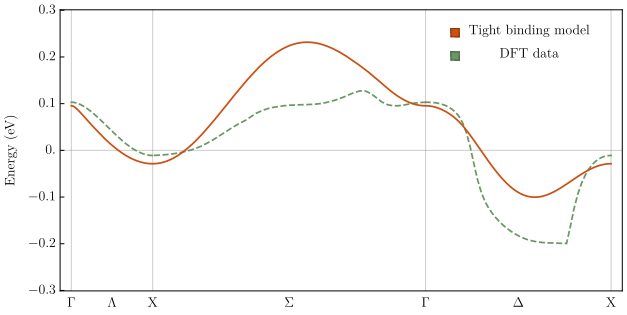

FIG. 10. Λ-Σ-Δ band dispersion of topological DFT calculation (U=1.2 eV) and the fitted TB model. The fit is for the TB model's lower band and weighted near FS. The TB band has roots close to the DFT roots.

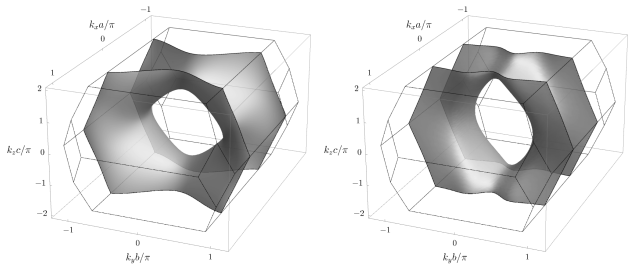

FIG. 11. 3D shapes of The FS. The left figure shows the FS of the fitted TB model and the right figure shows the FS of the DFT band.

[1] S. Ran, C. Eckberg, Q.-P. Ding, Y. Furukawa, T. Metz, S. R. Saha, I.-L. Liu, M. Zic, H. Kim, J. Paglione, and N. P. Butch, Science **365**, 684 (2019).

[2] D. Aoki, A. Nakamura, F. Honda, D. Li, Y. Homma, Y. Shimizu, Y. J. Sato, G. Knebel, J.-P. Brison, A. Pourret, D. Braithwaite, G. Lapertot, Q. Niu, M. Vališka, H. Harima, and J. Flouquet, Journal of the Physical Society of Japan **88**, 043702 (2019), https://doi.org/10.7566/JPSJ.88.043702.

[3] W. Knafo, M. Vališka, D. Braithwaite, G. Lapertot, G. Knebel, A. Pourret, J.-P. Brison, J. Flouquet, and D. Aoki, Journal of the Physical Society of Japan **88**, 063705 (2019), https://doi.org/10.7566/JPSJ.88.063705.

[4] A. Miyake, Y. Shimizu, Y. J. Sato, D. Li, A. Nakamura, Y. Homma, F. Honda, J. Flouquet, M. Tokunaga, and D. Aoki, Journal of the Physical Society of Japan **88**, 063706 (2019), https://doi.org/10.7566/JPSJ.88.063706.

[5] S. Imajo, Y. Kohama, A. Miyake, C. Dong, M. Tokunaga, J. Flouquet, K. Kindo, and D. Aoki, Journal of the Physical Society of Japan **88**, 083705 (2019), https://doi.org/10.7566/JPSJ.88.083705.

[6] V. P. Mineev, JETP Letters (2020), 10.1134/s0021364020120036.

[7] S. Ran, H. Kim, I.-L. Liu, S. R. Saha, I. Hayes, T. Metz, Y. S. Eo, J. Paglione, and N. P. Butch, Phys. Rev. B **101**, 140503(R) (2020).

[8] G. Knebel, M. Kimata, M. Vališka, F. Honda, D. Li, D. Braithwaite, G. Lapertot, W. Knafo, A. Pourret, Y. J. Sato, Y. Shimizu, T. Kihara, J.-P. Brison, J. Flouquet, and D. Aoki, Journal of the Physical Society of Japan **89**, 053707 (2020), https://doi.org/10.7566/JPSJ.89.053707.

[9] Q. Niu, G. Knebel, D. Braithwaite, D. Aoki, G. Lapertot, G. Seyfarth, J.-P. Brison, J. Flouquet, and A. Pourret, Phys. Rev. Lett. **124**, 086601 (2020).

[10] S. Ran, I.-L. Liu, Y. S. Eo, D. J. Campbell, P. M. Neves, W. T. Fuhrman, S. R. Saha, C. Eckberg, H. Kim, D. Graf, F. Balakirev, J. Singleton, J. Paglione, and N. P. Butch, Nature Physics **15**, 1250 (2019).

[11] S. Ikeda, H. Sakai, D. Aoki, Y. Homma, E. Yamamoto, A. Nakamura, Y. Shiokawa, Y. Haga, and Y. Ōnuki, Journal of the Physical Society of Japan **75**, 116 (2006).

[12] Y. Tokunaga, H. Sakai, S. Kambe, T. Hattori, N. Higa, G. Nakamine, S. Kitagawa, K. Ishida, A. Nakamura, Y. Shimizu, Y. Homma, D. Li, F. Honda, and D. Aoki, Journal of the Physical Society of Japan **88**, 073701 (2019), https://doi.org/10.7566/JPSJ.88.073701.

[13] S. Sundar, S. Gheidi, K. Akintola, A. M. Cote, S. R. Dunsiger, S. Ran, N. P. Butch, S. R. Saha, J. Paglione, and J. E. Sonier, Phys. Rev. B **100**, 140502(R) (2019).

[14] G. Nakamine, S. Kitagawa, K. Ishida, Y. Tokunaga, H. Sakai, S. Kambe, A. Nakamura, Y. Shimizu, Y. Homma, D. Li, F. Honda, and D. Aoki, J. Phys. Soc. Jpn. **88**, 113703 (2019).

[15] D. Braithwaite, M. Valiska, G. Knebel, G. Lapertot, J.-P. Brison, A. Pourret, M. E. Zhitomirsky, J. Flouquet, F. Honda, and D. Aoki, Communications Physics **2**, 147 (2019).

[16] I. M. Hayes, D. S. Wei, T. Metz, J. Zhang, Y. S. Eo, S. Ran, S. R. Saha, J. Collini, N. P. Butch, D. F. Agterberg, A. Kapitulnik, and J. Paglione, "Weyl superconductivity in UTe_2," (2020), arXiv:2002.02539 [cond-mat.str-el].

[17] S. M. Thomas, F. B. Santos, M. H. Christensen, T. Asaba, F. Ronning, J. D. Thompson, E. D. Bauer, R. M. Fernandes, G. Fabbris, and P. F. S. Rosa, "Evidence for a pressure-induced antiferromagnetic quantum critical point in intermediate valence UTe_2," (2020), arXiv:2005.01659 [cond-mat.str-el].

[18] K. Machida, Journal of the Physical Society of Japan **89**, 033702 (2020), https://doi.org/10.7566/JPSJ.89.033702.

[19] S. Kittaka, Y. Shimizu, T. Sakakibara, A. Nakamura, D. Li, Y. Homma, F. Honda, D. Aoki, and K. Machida, Phys. Rev. Research **2**, 032014 (2020).

[20] S. Bae, H. Kim, S. Ran, Y. S. Eo, I.-L. Liu, W. Fuhrman, J. Paglione, N. P. Butch, and S. Anlage, "Anomalous normal fluid response in a chiral superconductor," (2019), arXiv:1909.09032 [cond-mat.supr-con].

[21] L. Jiao, S. Howard, S. Ran, Z. Wang, J. O. Rodriguez, M. Sigrist, Z. Wang, N. P. Butch, and V. Madhavan, Nature **579**, 523 (2020).

[22] D. Aoki, K. Ishida, and J. Flouquet, J. Phys. Soc. Jpn. **88**, 022001 (2019).

[23] A. B. Shick and W. E. Pickett, Phys. Rev. B **100**, 134502 (2019).

[24] Y. Xu, Y. Sheng, and Y.-F. Yang, Phys. Rev. Lett. **123**, 217002 (2019).

[25] J. Ishizuka, S. Sumita, A. Daido, and Y. Yanase, Phys. Rev. Lett. **123**, 217001 (2019).

[26] A. A. Soluyanov and D. Vanderbilt, Phys. Rev. B **83**, 035108 (2011).

[27] T. Metz, S. Bae, S. Ran, I.-L. Liu, Y. S. Eo, W. T. Fuhrman, D. F. Agterberg, S. Anlage, N. P. Butch, and J. Paglione, Phys. Rev. B **100**, 220504(R) (2019).

[28] S.-i. Fujimori, I. Kawasaki, Y. Takeda, H. Yamagami, A. Nakamura, Y. Homma, and D. Aoki, Journal of the Physical Society of Japan **88**, 103701 (2019), https://doi.org/10.7566/JPSJ.88.103701.

[29] L. Miao, S. Liu, Y. Xu, E. C. Kotta, C.-J. Kang, S. Ran, J. Paglione, G. Kotliar, N. P. Butch, J. D. Denlinger, and L. A. Wray, Phys. Rev. Lett. **124**, 076401 (2020).

[30] M. Weinert, G. Schneider, R. Podloucky, and J. Redinger, J. Phys. Condens. Matter **21**, 084201 (2009).

[31] A. N. Yaresko, V. N. Antonov, and P. Fulde, Phys. Rev. B **67**, 155103 (2003).

[32] L. Fu and C. L. Kane, Phys. Rev. B **76**, 045302 (2007).

[33] T. H. Hsieh and L. Fu, Phys. Rev. Lett. **108** (2012).

[34] K. Miyake, S. Schmitt-Rink, and C. M. Varma, Phys. Rev. B **34**, 6554 (1986).

[35] D. J. Scalapino, Rev. Mod. Phys. **84**, 1383 (2012).

[36] A. Ramires and M. Sigrist, Phys. Rev. B **94**, 104501 (2016).

[37] A. Ramires, D. F. Agterberg, and M. Sigrist, Phys. Rev. B **98**, 024501 (2018).

[38] V. G. Yarzhemsky and E. A. Teplyakov, "Time-reversal symmetry and the structure of superconducting order Parameter of nearly ferromagnetic spin-triplet superconductor UTe_2," (2020), arXiv:2001.02963 [cond-mat.supr-con].

[39] A. H. Nevidomskyy, "Stability of a nonunitary triplet pairing on the border of magnetism in UTe_2," (2020), arXiv:2001.02699 [cond-mat.supr-con].

[40] D. Aoki, F. Honda, G. Knebel, D. Braithwaite, A. Nakamura, D. Li, Y. Homma, Y. Shimizu, Y. J. Sato, J.-P. Brison, and J. Flouquet, Journal of the Physical Society of Japan **89**, 053705 (2020).

[41] W.-C. Lin, D. J. Campbell, S. Ran, I.-L. Liu, H. Kim, A. H. Nevidomskyy, D. Graf, N. P. Butch, and J. Paglione, "Tuning magnetic confinement of spin-triplet superconductivity," (2020), arXiv:2002.12885 [cond-mat.supr-con].

[42] E. Lange and G. Kotliar, Phys. Rev. Lett. **82**, 1317 (1999).

[43] P. M. R. Brydon, D. F. Agterberg, H. Menke, and C. Timm, Phys. Rev. B **98**, 224509 (2018).

[44] P. M. R. Brydon, D. S. L. Abergel, D. F. Agterberg, and V. M. Yakovenko, Phys. Rev. X **9**, 031025 (2019).

[45] E. Taylor and C. Kallin, Phys. Rev. Lett. **108**, 157001 (2012).